Ponderomotive Pseudopotential Near Gyroresonance

Guy Dimonte, B. M. Lamb, and G. J. Morales

Physics Department, University of California at Los Angeles, Los Angeles, California 90024

The enhancement of the ponderomotive potential near gyroresonance is investigated both experimentally and theoretically. Because of nonadiabaticity near gyroresonance the potential is finite and depends on the transit time of the particle through the rf field structure.

It is known that a spatially localized rf electric field $\vec{E}$ of frequency ω produces an average static force, i.e., a ponderomotive force.[1] In the presence of a static magnetic field $\vec{B}$ a large enhancement of the ponderomotive force is predicted[2] to appear as ω approaches the particle gyrofrequency Ω. The standard expression[2] given for the ponderomotive pseudopotential is

$$\varphi_p = q^2|\vec{E}|^2/4m(\omega^2 - \Omega^2),\qquad(1)$$

where q and m are the charge and mass of the particle. The nonphysical singularity in Eq. (1) arises because in obtaining this expression the gradient scale length l of the electric field is assumed to be large compared to $v/(\omega - \Omega)$, where v is the unperturbed particle velocity. However, this adiabatic approximation[3] is not valid near gyroresonance, and hence the singularity in Eq. (1) is suspect. Indeed, for $\omega \approx \Omega$ the particles do not respond adiabatically and are instead resonantly heated. Since the ponderomotive force plays a fundamental[4] role in many nonlinear processes in plasma physics, it is important to understand the singular behavior near the gyrofrequency. In particular, efforts are in progress to utilize the singular nature of φ_p to selectively confine ions of different q/m for isotope separation[5,6] and to plug open-ended confinement systems.[7,8]

In this Letter, we present measurements of the ponderomotive potential near gyroresonance and compare them with a calculation which includes nonadiabatic effects. It is found, both experimentally and theoretically, that φ_p is small at $\omega = \Omega$ rather than singular. In fact, the maximum enhancement in φ_p does not occur at $\omega = \Omega$, but at the transition from the nonadiabatic to the adiabatic regime, namely, when $\omega \approx \Omega + 1.7v/l$. In the nonadiabatic regime strong heating is observed primarily perpendicular to $\vec{B}$.

The experiment is performed by injecting a low-density (single-particle limit) monoenergetic pulse of ions through an electrostatic rf structure

as shown in Fig. 1. The rf electric field amplitude is increased until the transmitted current disappears. At this point φ_p is equal to the kinetic energy $mv^2/2$ of the particles. The ion source is a thermionic[7] Li$^+$ emitter[9] which is biased to a positive potential V_s. A pulse of ions of energy qV_s is produced by gating a grid from $V > V_s$ to $V = 0$ for a duration of 20 μs. The ions are guided along the axis of a grounded conducting cylinder by a uniform axial magnetic field $B_0 = 1.8$ kG. The beam radius is 0.5 cm, and the cylinder radius is 7.3 cm. The rf antenna consists of two electrically isolated electrodes made by splitting a cylinder in half lengthwise. It is excited through a center-tapped transformer so that $\vec{E}$ is perpendicular to $\vec{B}$ on axis. We have calculated the vacuum rf field $\vec{E}(r,z)$ analytically to relate $\vec{E}$ to the rf potential $\pm V_{rf}$ applied to the electrodes. On axis, the field can be approximated by a Gaussian profile $\vec{E}(0,z) = \hat{y}E_0\exp(-z^2/2l^2)$ with scale length l which can be varied by changing the length of the antenna. The ions which pass through the antenna are collected by an electrode which is 137 cm away from the source.

The ponderomotive potential is measured for a fixed value of ω, Ω, l, and v by increasing V_{rf} until the transmitted ion current disappears. For this value of V_{rf} the ponderomotive potential equals the initial kinetic energy. If the gyrofrequency enhancement of the ponderomotive poten-
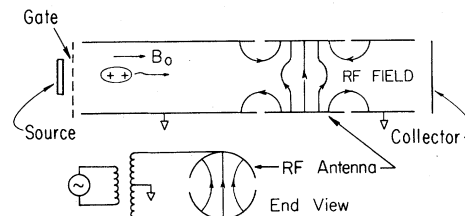
FIG. 1. Schematic of the experiment.

tial is large then a relatively small rf electric field is required to reflect the particles and vice versa. For frequencies near the gyrofrequency, strong cyclotron heating occurs and particles can be collected on the antenna if the gyroradius is large. In order to insure that the decrease in the transmitted ion current is due to the ponderomotive force, the reflected particles are electrostatically reflected again at the gate grid and collected for analysis by turning off the rf voltage. Only data with a significant fraction of reflected particles are reported here. The initial kinetic energy of the ions is $qV_s \pm 15\%$ as verified by time-of-flight analysis and retarding-field analyzer measurements. The electric field amplitude on axis E_0 is obtained from V_{rf} by using our analytical solutions for the vacuum field. This is justified because the ion density ($< 2 \times 10^5$ cm^{-3}) is purposely small to minimize space-charge effects. The gradient scale length l is also obtained from these calculations since the antenna radius and length are known.

Figure 2 shows the behavior of the ponderomotive potential near the gyrofrequency. φ_p is scaled to $q^2 E_0^2 / 4m\Omega^2$ as suggested by Eq. (1) to facilitate comparison of the data (points) with the theoretical predictions (solid curves). The curve for $v/l\Omega = 0$ is given by Eq. (1) and the rest will be described later. Five sets of data for different values of l and v are shown to demonstrate the important parametric dependences. Away from gyroresonance φ_p agrees quantitatively with the prediction of Eq. (1) whereas near Ω the data disagree even qualitatively; φ_p reaches a maximum at a frequency greater than Ω and tends toward a small value at Ω. There are three sets of data which have the same value of $v/l\Omega$ but different values of l and v. These data agree with one another within the experimental error indicating that the relevant parameter is $v/l\Omega$. By obtaining data over a wide range of parameters, we find that the maximum in φ_p occurs at a frequency $\omega \approx \Omega + 1.7v/l$. As a result, the maximum enhancement of the ponderomotive potential depends on various parameters through the figure of merit $v/l\Omega$; the implication is that in order to obtain a significant enhancement of the ponderomotive force near gyroresonance $v/l\Omega$ must be small.

To explain these results it is necessary to integrate the equation of motion properly as a particle traverses an electric field structure of finite extent. Consider the exact equation of motion for a particle with position $\vec{r}$ in the magnetic
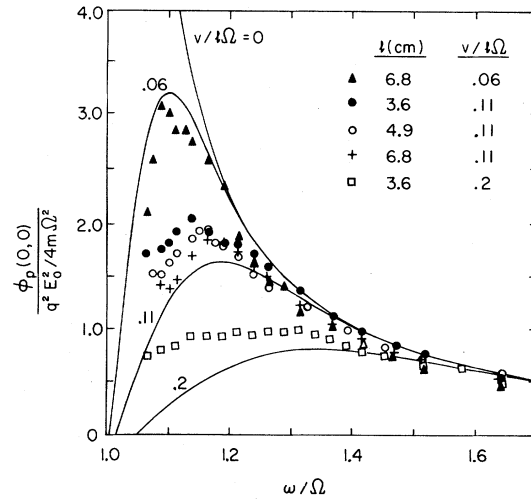
FIG. 2. Scaled ponderomotive potential vs frequency for different conditions. The points are measurements and the curves are the theoretical predictions. The curve for $v/l\Omega = 0$ is given by Eq. (1).

field $\vec{B} = B_0 \hat{z}$,

$$\ddot{\vec{r}} = (q/m)\vec{E}(\vec{r},t) + \Omega \dot{\vec{r}} \times \hat{z}. \tag{2}$$

For simplicity, assume that $\vec{E} = [E_y(y,z)\hat{y} + E_z(y,z)\hat{z}]\cos(\omega t + \psi)$, where ψ is a phase factor and $\nabla \times \vec{E} = 0$. We proceed to solve Eq. (2) by employing a multiple-time-scale perturbation expansion $\vec{r}(t) = \vec{r}_s(t) + \vec{r}_f(t)$, where $\vec{r}_f$ gives the fast response of the particle and $\vec{r}_s$ varies on slow time scale (compared to $2\pi/\omega$). By expanding $\vec{E}(\vec{r},t)$ about $\vec{r}_s$ assuming $|\vec{r}_f| \ll l$ and equating terms on similar time scales, we obtain

$$\ddot{\vec{r}}_f = (q/m)\vec{E}(\vec{r}_s,t) + \Omega \dot{\vec{r}}_f \times \hat{z}, \tag{3}$$

where $\vec{E}(\vec{r}_s,t)$ is evaluated at the average location $\vec{r}_s$. The slow response of the particle is determined by the static ponderomotive force

$$F_p = q\langle (\vec{r}_f \cdot \nabla)\vec{E}(\vec{r}_s,t)\rangle, \tag{4}$$

where the angular brackets denote an average over the fast time scale $2\pi/\omega$. The parallel component responsible for stopping the particle has two contributions, $\langle qy_f \, dE_z/dy \rangle$ and $\langle qz_f \, dE_z/dz \rangle$. The latter gives the usual unmagnetized contribution[1] which is not of interest here and is quite small in our experiment because $E_z = 0$ on axis ($y = 0$) where the particles are injected. With $\nabla \times \vec{E} = 0$ the first term becomes $\langle qy_f \, dE_y/dz \rangle$. To evaluate this we solve for y_f by integrating Eq.

(3),

$$y_f = (q/m\Omega)\int_{-\infty}^{t} dt' E_y[0,z_s(t')]\sin[\Omega(t-t')]\cos(\omega t' + \psi). \tag{5}$$

In the adiabatic limit $l(\omega - \Omega)/v \gg 1$, $E_y(0,z_s)$ can be removed from the integral, y_f becomes singular, and the standard result, i.e., Eq. (1), is recovered. However, near gyroresonance E_y must be retained inside the time history integral. In general, Eq. (5) is difficult to solve, and hence we make the simplification that $z_s(t) = vt$. That is, we integrate over the unperturbed particle orbit retaining E_y inside the integral. We shall return to this point later. Substituting y_f into Eq. (4) and defining the ponderomotive pseudopotential as $\varphi_p(0,z) \equiv -\int_{-\infty}^{z} dz' \vec{F}_p(0,z') \cdot \hat{z}$ we obtain

$$\varphi_p(0,z) = \frac{q^2}{8m\Omega v} \sum_{n=\pm 1} \left(2E_y(0,z)\mathrm{Im}\epsilon_n(z) + \frac{(\Omega + n\omega)}{v}|\epsilon_n(z)|^2 \right), \tag{6}$$

where Im refers to the imaginary part and

$$\epsilon_n(z) \equiv \int_{-\infty}^{z} dz' E_y(0,z')\exp[i(\Omega + n\omega)(z' - z)/v], \quad n = \pm 1. \tag{7}$$

In the adiabatic limit $(\omega - \Omega)l/v \gg 1$, Eq. (6) reduces to Eq. (1). Otherwise the strength of the potential has an additional dependence on the electric field profile and the velocity of the particle.

Use of a Gaussian profile for E_y in Eq. (7) gives an analytical expression for $\varphi_p(0,z)$ in terms of the plasma dispersion function.[10] Proceeding to identify $\varphi_p(0,0)$ with the maximum stopping power measured in the experiment, one arrives at the solid curves exhibited in Fig. 2. The calculations agree well with the experimental data. This result also explains previous rf plugging experiments,[7,8] in which the maximum ponderomotive stopping occurred at frequencies above the gyrofrequency, without having to invoke collective effects.

In obtaining Eq. (6) it is assumed that the particle orbit is unperturbed. In order to understand the error associated with this approximation when applied to reflected particles we have compared the analytical calculation with results of exact numerical solutions to the equation of motion. For each value of $v/l\Omega$ we solved Eq. (2) numerically for thirty values of the phase factor ψ between 0 and 2π. The electric field used corresponds to the Gaussian profile described previously. Numerically the ponderomotive potential is obtained by computing the phase-averaged decrease in kinetic energy at $z = 0$.

Representative numerical results are shown in Fig. 3. The solid curve is the same analytical calculation shown in Fig. 2 for $v/l\Omega = 0.11$. The points are calculated numerically for two amplitudes of the electric field. For the solid points E_0 is small and the particle orbits are barely perturbed. As expected the agreement with the perturbation calculation is excellent. For the circles the electric field amplitude is increased

just enough to reflect the particles at each frequency. Here the maximum in φ_p is slightly larger by 17% than that predicted by Eq. (6) and occurs slightly closer to the gyrofrequency in agreement with the experimental data in Fig. 2 for $v/l\Omega = 0.11$. The behavior of φ_p is characteristic of a particle with a slightly smaller unperturbed velocity than the initial $v = 0.11l\Omega$. Physically this is expected because near the reflection point the particle moves more slowly and therefore samples a larger force than estimated when using the unperturbed trajectory. Similar results have been obtained for different values of $v/l\Omega$. They all indicate that the use of unperturbed orbits causes a slight underestimate of the poten-
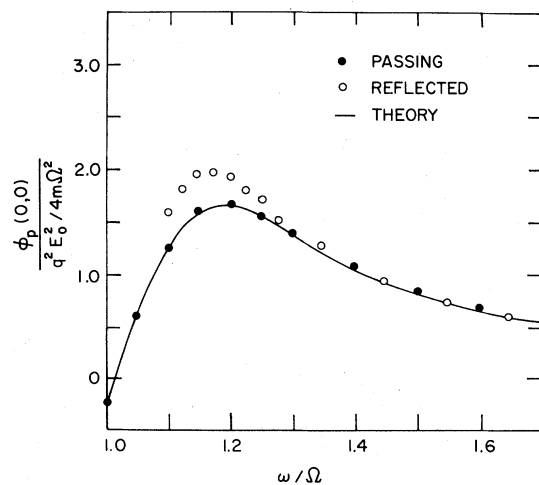
FIG. 3. Scaled ponderomotive potential vs frequency for $v/l\Omega = 0.11$. The curve is the analytical result and the points are obtained numerically for passing and reflected particles.

tial for reflected particles because their average velocity is smaller than the initial velocity. Nevertheless, the simple analytical calculation predicts the salient results to an accuracy better than 20% and indicates the important scaling dependence on $v/l\Omega$. In applications where a (15–20)% change is acceptable the perturbation calculation is more useful and instructive than the tedious numerical solution.

In summary, a second-order perturbation calculation illustrates the finite nature of the ponderomotive effect near the gyroresonance and agrees with detailed experimental observations and numerical calculations with test ions. Near the gyrofrequency the ponderomotive pseudopotential is a function not only of position but also depends on the velocity of the particles. Physically, this occurs when the transit time l/v is short compared to the time required for the particle to see a change in the phase of the electric field, i.e., $(\omega - \Omega)^{-1}$. In the nonadiabatic regime, the notion of a time-independent force breaks down and stochastic heating occurs.[11] Since adiabaticity is intrinsic to the ponderomotive force its role must be considered in any realistic application.

We would like to thank Rudy Salazar for his ex-

[1]A. V. Gaponov and M. A. Miller, Zh. Eksp. Teor. Fiz. 34, 242 (1958) [Sov. Phys. JETP 7, 168 (1958)].

[2]L. P. Pitaevskii, Zh. Eksp. Teor. Fiz. 39, 1450 (1960) [Sov. Phys. JETP 12, 1008 (1961)].

[3]A. J. Lichtenberg and H. L. Berk, Nucl. Fusion 15, 999 (1975).

[4]J. R. Cary and A. N. Kaufman, Phys. Fluids 24, 1238 (1981).

[5]S. Hidekuma, S. Hiroe, T. Watari, T. Shoji, T. Sato, and K. Takayama, Phys. Rev. Lett. 33, 1537 (1974).

[6]E. S. Weibel, Phys. Rev. Lett. 44, 377 (1980).

[7]S. Hiroe, S. Hidekuma, T. Watari, T. Shoji, T. Sato, and K. Takayama, Nucl. Fusion 15, 769 (1975).

[8]T. Watari, T. Hatori, R. Kumazawa, S. Hidekama, T. Aoki, T. Kawamoto, M. Inutake, S. Hiroe, A. Nishizawa, K. Adati, T. Sato, T. Watanabe, H. Obayashi, and K. Takayama, Phys. Fluids 21, 2076 (1978).

[9]G. Dimonte, Phys. Rev. Lett. 46, 26 (1981).

[10]B. D. Fried and S. Conte, The Plasma Dispersion Function (Academic, New York, 1961).

[11]G. J. Morales and Y. C. Lee, Phys. Rev. Lett. 33, 1534 (1974).

Nonlinear Evolution of the Ion-Ion Beam Instability

H. L. Pécseli

Association EURATOM, Risø National Laboratory, DK-4000 Roskilde, Denmark

and

J. Trulsen

Institute of Mathematical and Physical Sciences, University of Tromsø, N-9001 Tromsø, Norway

The criterion for the existence of vortexlike ion phase-space configurations, as obtained by a standard pseudopotential method, is found to coincide with the criterion for the linear instability for two (cold) counterstreaming ion beams. A nonlinear equation is derived, which demonstrates that this instability actually evolves into such phase-space configurations. A small, but nonzero, ion temperature turns out to be essential for the saturation into stationary structures.

PACS numbers: 52.35.Py

Numerical simulations[1] demonstrated that electron-electron two-stream instabilities evolve into rather stable vortexlike phase-space structures (also called electron holes[2]). Such equilibrium configurations were subsequently observed in a laboratory experiment.[3] Numerical solutions of the ion Vlasov equation,[4] under the assumption of isothermally Boltzmann distributed electrons, demonstrated that similar structures could evolve also in ion phase space, in connection with the formation of ion-acoustic shocks. Also this result found experimental confirmation.[5] A unified